Bull Volcanol (2002) 64:363–371
DOI 10.1007/s00445-002-0213-6

RESEARCH ARTICLE

C. Buisson · O. Merle

Experiments on internal strain in lava dome cross sections

Received: 9 March 2001 / Accepted: 8 March 2002 / Published online: 18 June 2002

Abstract Simple experiments have been conducted to study the strain evolution in lava dome cross sections. A viscous fluid is injected vertically from a reservoir into a feeding conduit. Silicone putty is used as analogue magma. Two-dimensional experiments allow the assessment of the internal strain within the dome. Particle paths are symmetrical on either side of a central line passing through the feeding conduit and display parabolic trajectories. The highest strain zone is located above the extrusion zone. In cross sections, stretch trajectories show a remarkable concentric pattern, wrapping around the extrusion zone of the analogue magma. To the lateral margins, a triple junction of stretch trajectories defines an isotropic point in the strain field. In the main central part of the dome, an intermediate zone of reversed sense of shearing is caused by a change in the sign of the velocity gradient with respect to that in the upper and lower zones. Knowledge of this evolving strain pattern can provide a better understanding of the evolution of natural domes. Also, it can help to unravel the kinematic history of ancient domes partly removed by erosion.

Keywords Analogue modelling · Domes emplacement · Kinematic evolution · Particle paths · Stretch trajectories

Editorial responsibility: D. Dingwell

C. Buisson (✉)
Laboratoire Magmas et Volcans,
Observatoire de Physique du Globe,
CNRS – Université Blaise Pascal,
5 rue Kessler, 63038 Clermont-Ferrand, France
e-mail: C.Buisson@opgc.univ-bpclermont.fr
e-mail: cecile.buisson@laposte.net
Tel.: +33-4-73346721, Fax: +33-4-73346744

O. Merle
Laboratoire Magmas et Volcans,
Observatoire de Physique du Globe,
CNRS – Université Blaise Pascal,
5 rue Kessler, 63038 Clermont-Ferrand, France

Introduction

Studies of dome growth are abundant (e.g. Williams 1932; Christiansen and Lipman 1966; Cole 1970; Huppert et al. 1982; Murase et al. 1985; Fink and Manley 1987; Swanson et al. 1987; Anderson and Fink 1990; Duffield and Dalrymple 1990; Swanson and Holcomb 1990; Dadd 1992; Miller 1994; Fink and Bridges 1995; Nakada et al. 1995). These mostly deal with the mechanical aspects of lava dome emplacement. These studies have brought much information about the evolution of height vs. diameter, flow vs. extrusion rate, and the rheology of the magma during emplacement, which constitute an invaluable source of data.

Huppert et al. (1982) were the first to present analogue models concerning lava dome growth. They used a simple Newtonian fluid flowing radially under its own hydrostatic pressure on a horizontal surface. They compared experimental results with the growth of the St Vincent Soufriere dome.

Over the past decade, several studies have described experiments of lava domes. Blake (1990) introduced non-Newtonian effects using Bingham slurries of kaolin and water. According to observed changes in aspect ratios, Blake proposed four classes of domes: upheaved plugs, pelean, low and coulee.

Experiments using kaolin slurry injected in to cold water (Griffiths and Fink 1993, 1997) or gum resin (Lejeune 1995) have allowed a better understanding of the cooling effect on lava dome evolution. Fink and Bridges (1995) emplaced polyethylene glycol (PEG) wax into cold sucrose to study the impact of eruption history and cooling rate on lava dome growth. These studies have dealt with the geometrical aspects of domes, including the evolution of the height/diameter ratio with time and the varying textures at the surface of the dome during cooling. They have stressed the physical constraints leading to dome collapse and explosion, and have investigated their consequences on the dynamics of eruptive processes.

Field data on the evolving strain within endogenous lava domes are scarce. This is mainly for two reasons:

Table 1 List of experiments carried out in this study

Experiment	Type	Effusion rate ($cm^3\ h^{-1}$)	Duration (h)	Marker type	Material
1	3-D	0.26	80	Tinted wood particles	Transparent silicone
2	3-D	0.54	72.5	Tinted wood particles	Transparent silicone
3	3-D	0.78	60	Tinted wood particles	Transparent silicone
4	3-D	1.04	60	Tinted wood particles	Transparent silicone
5	3-D	1.30	55	Tinted wood particles	Transparent silicone
6	2-D	0.26	80	Tinted wood particles	Transparent silicone
7	2-D	1.30	56	Tinted wood particles	Transparent silicone
8	2-D	0.26	80	Tinted wood particles	Transparent silicone Non-lubricated walls
9	2-D	0.26	80.5	Small coloured sticks	Transparent silicone
10	2-D	2.6	53	Small coloured sticks	Transparent silicone
11	2-D	2.6	7	5-mm grid	Pink silicone
12	2-D	2.6	7.75	5-mm grid	Pink silicone
13	2-D	2.6	22	5-mm grid	Pink silicone
14	2-D	2.6	7.5	5-mm grid	Pink silicone
15	2-D	2.6	7	5-mm grid	Pink silicone
16	2-D	2.6	7	3-mm grid	Pink silicone
17	2-D	2.6	6	3-mm grid	Pink silicone
18	2-D	2.6	7.75	3-mm grid	Pink silicone
19	2-D	2.6	8	3-mm grid	Pink silicone
20	3-D	2.6	23.25	3- and 5-mm grid	Pink silicone
21	2-D	0.26	46	3-mm grid	Pink silicone

either the dome was active and direct observations of the deforming interior was not possible or the dome was cooled and erosion reveals only the final stage of deformation. This is why little is known about their overall internal strain.

To address this question, simple experiments have been conducted with a viscous fluid, injected vertically and flowing on a rigid planar base. The scaled models reveal the internal strain patterns that can be expected in viscous endogenous domes. They make it possible to determine particle paths, velocity gradients, sense of shearing and the attitude of the flattening plane.

Experimental procedure

In our experiments, silicone is poured into a reservoir and simulates viscous magma (Fig. 1). Pushed up by a piston, the silicone is vertically extruded through a feeding conduit of 6 mm in diameter and flows on a rigid planar base. The velocity of the piston is governed by a computer-controlled stepper motor and the silicone comes out of the feeding conduit at a rate ranging from 0.26–2.6 $cm^3\ h^{-1}$ (Table 1).

In three-dimensional experiments, the silicone spreads radially onto a horizontal base exhibiting a symmetrical deformation pattern around an axis corresponding to the feeding conduit.

In two-dimensional experiments, the viscous fluid is confined between two walls of glass 6 mm apart corresponding to the width of the feeding conduit. These 2-D models make it possible to study internal strain and motion. When using transparent silicone, particle paths within the dome are followed by the means of small elongated pieces of wood previously incorporated into the reservoir. When using pink silicone, a square grid of

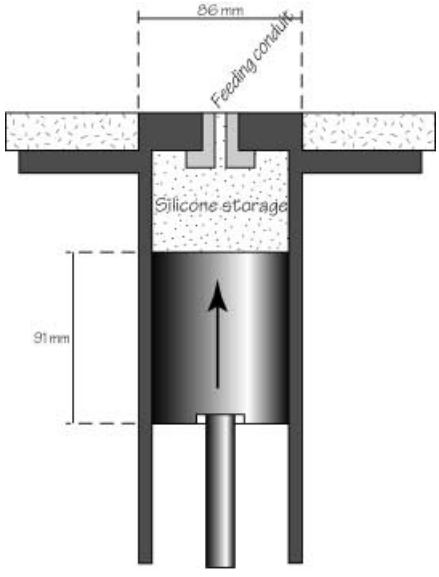

Fig. 1 Experimental device – the feeding conduit is 6 mm wide

carbon is printed on the lateral side once the extruding silicone has risen up enough to exhibit an hemi-elliptical shape of a few centimetres high (i.e. 5 or 6 h after the beginning of the experiment; Fig. 2b, c). The grid is emplaced by removing one of the two walls for a few seconds. At the same time, the glass is lubricated with a soap mixture in order to avoid boundary effects. The lubricated walls cause the silicone to glide freely and no boundary effect was observed. Because of this experimental procedure, two-dimensional experiments only reveal the evolution of mature domes because the first stages of deformation cannot be investigated.

During experiments, successive photographs of the deforming grid or particle trajectories are taken through

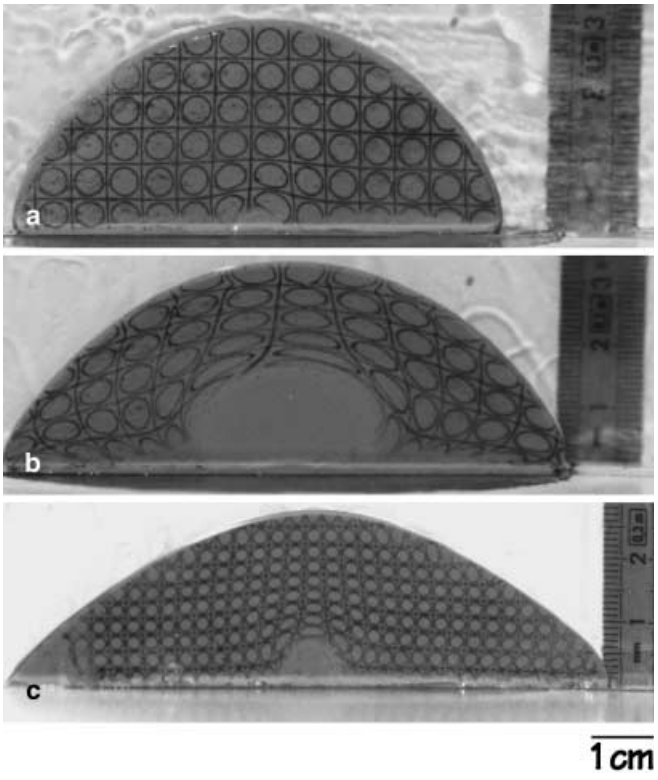

Fig. 2a–c Photographs of two-dimensional experiments. **a**, **b** Experiment 15 at an injection rate of 2.6 $cm^3\ h^{-1}$. The deformation (*bottom*) of initially undeformed square grid (*top*) allows computation of strain anywhere in the model except in the lower central zone of newly injected material. **c** Deformation of a grid with smaller square and circle elements in experiment 21 after a duration of 41 h, 30 min after grid emplacement.

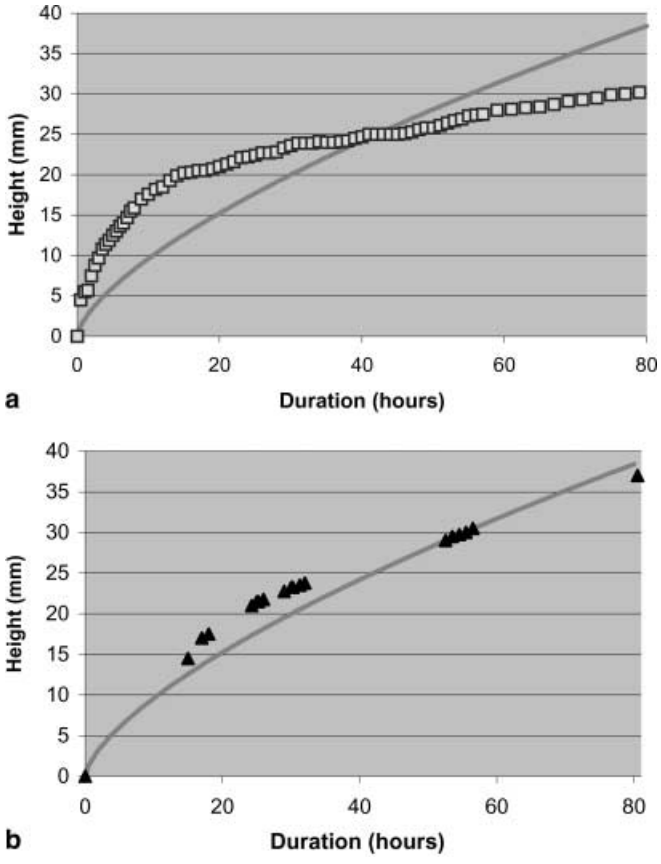

Fig. 3 Height versus time in a slot and in 2-D experiments with **a** lubricated and **b** non-lubricated walls. *Squares* and *triangles* represent experimental data in lubricated and non-lubricated experiments 6 and 8, respectively. *Solid line* is the height evolution in a slot according to the theoretical equation

the glass to follow the evolving strain pattern. Experiments have been conducted at room temperature and have lasted from 6 to 80 h.

Our experiments are intended to be geometrically, kinematically and dynamically similar to natural domes (Hubbert 1937; Ramberg 1981; Merle and Borgia 1996). As the model uses an isothermal Newtonian fluid, the only criterion that is relevant for justifying the experiments as analogues of the volcanic flows is that the Reynolds numbers are small in both cases. The Reynolds number is :

$$Re = \rho\, HR/\mu t$$

where H and R are the height and the radius of the dome.

The Reynolds number varies from 10^{-9} to 10^{-11} in experiments and is about 5×10^{-11} in nature. These very small values (Re $<<1$) indicate that inertial forces are negligible with respect to viscous forces both in nature and experiments.

To be sure that 2-D experiments, despite the lubrication procedure, do not show the pattern of deformation in a slot flow, we have compared the evolution of the height in experiments with that expected in a slot according to theoretical equations (Blake, personal communication).

In a slot flow, the height is given by :

$$H = (q^2\mu/\rho g L^2)^{1/3} t^{1/3}$$

where L is the width of the slot and q the flow rate per unit width.

Figure 3a shows that the height in a slot is continuously increasing whereas it is asymptotic to an upper value in experiments. On the other hand, when non-lubricated walls are used in control experiments, the height does continuously increase (Fig. 3b).

Relevance of experiments using an isothermal Newtonian fluid

As pointed out by many authors (Blake 1990; Griffiths and Fink 1993; Fink and Bridges 1995; Griffiths and Fink 1997), the magma in natural domes does not behave as a Newtonian fluid and is best described as a temperature-dependent Bingham material with a yield stress τ. This is why recent experiments on lava domes have used sophisticated apparatus with Bingham slurries in order to determine the effect of the yield stress on magma behaviour (Blake 1990; Griffiths and Fink 1997).

The goal of this paper is to investigate internal strain during the dome growth, which is mainly the attitude of the flattening plane, the sense of shear, the particle path and the velocity gradient as observed in cross section. A few studies have shown particle path and deformation observed at the surface of the dome (Blake 1990), but we are not aware of data about internal strain in cross section deduced from numerical or experimental analyses. Studying deformation within the dome needs to use a different experimental procedure where the strain pattern could be observed and followed with time from square grids emplaced upon the analogue material in section. To do so, we had to return to the simplest material because such a procedure can be done with isothermal Newtonian fluids as silicone putty and not with Bingham slurries. These experiments should be considered as a preliminary approach to studying internal strain within a dome and the results should be handled with care.

However, it is doubtless that previous studies using Newtonian isothermal fluids and that have been devoted to mechanical aspects of lava dome emplacement have led to a better understanding of these volcanic flows (i.e. Huppert et al. 1982; Fink and Griffith 1990). Starting from scratch (or nearly so), scale modelling of the strain pattern in vertical cross sections using a Newtonian fluid is likely to give a basic estimate of the evolving internal strain within a dome, which will be refined when more appropriate experimental procedures will be implemented.

It is interesting to evaluate if the dome shape evolution in our model matches that observed in nature. To verify this point, diameters have been measured either directly during the dome growth or later from photos taken during the experiment.

Results may first be compared with the St Vincent Soufrière dome. Huppert et al. (1982) gave an empirical relation between the dome radius (R) and time (t) based on natural observations during the growth of this dome (Fig. 4):

$$R = 0.051t^{0.580}$$

This equation reveals a radius evolution, which is similar to that observed in experiments at high injection rates (0.78 and 1.04 cm^3/h; Fig. 4).

We believe significant that the diameter evolution in experiments fits that observed in nature. This strongly suggests that displacement and motion of silicone within the scaled models are similar to the overall flow of magma in a natural dome. If this hypothesis is correct, strain pattern resulting from particle paths in experiments is likely to be close to internal strain in nature.

However, our experiments do not incorporate an upper solidified crust because of the cooling down of the fresh magma at the surface. Such a crust may modify the strain pattern in the vicinity of the upper rigid boundary where shear stresses should act along the contact. This other limitation of the model must be kept in mind when comparing experimental results with natural observations.

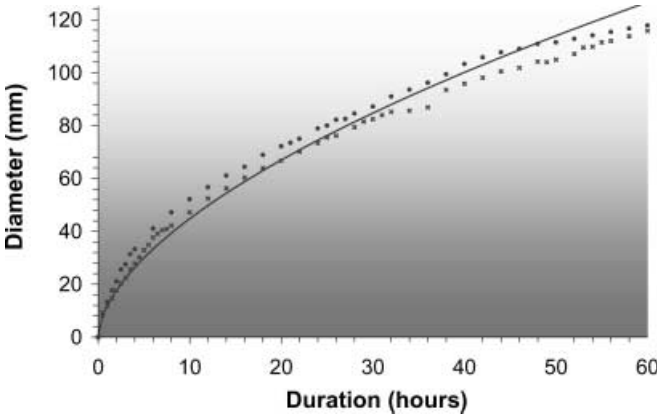

Fig. 4 Diameter of dome versus duration of experiments in 3-D models. Data for experiments at a rate of injection of 0.78 cm^3 h^{-1} (*crosses* experiment 3) and 1.04 cm^3 h^{-1} (*circles* experiment 4) fit the empirical curve derived by Huppert et al. (1982) from natural data at the dome of St Vincent Soufriere (*solid line*)

Particle paths

Particle paths are reconstructed both from the motion of small pieces of sugar or wood embedded into the transparent silicone and from the motion of each node of the square grid emplaced on the surface of the pink silicone.

On a map view (Fig. 5a), trajectories are radial, regardless of the vertical position of the particles within the dome. Varying the injection rates does not change this radial pattern of displacement, already observed in experiments using Bingham materials (Blake 1990). Once a given particle reaches the front, it becomes involved in the rolling of the upper free surface, which is the typical motion of spreading materials already described in experiments on nappe tectonics (Bucher 1956; Merle 1986) or lava flows (Merle 1998).

In vertical cross sections, trajectories are parabolic and symmetric on both sides of a vertical line located above the feeding conduit. Two types of particle paths can be described according to the position of the particle within the feeding conduit at the time when they are vertically extruded (Fig. 5b, c). Particles extruded from the lateral sides of the feeding conduit exhibit a slight rising trajectory, which subsequently becomes nearly horizontal or even downward as particles move towards the dome margin. In a way similar to observations at the upper free surface, particles move down when approaching the margins to be involved in the frontal rolling.

In contrast, particles extruded from the central part of the feeding conduit exhibit first a strong vertical component of motion. In this zone, particles move faster than those previously considered. Vertical motion of the particles and the vertical and lateral extent of this area increases with the injection rate.

The strong vertical component of motion in the central zone must be a result of the injection force, which locally overcomes the gravity force. The lower peripheral area, which reveals nearly horizontal or down-going movements, would be mainly dominated by gravity.

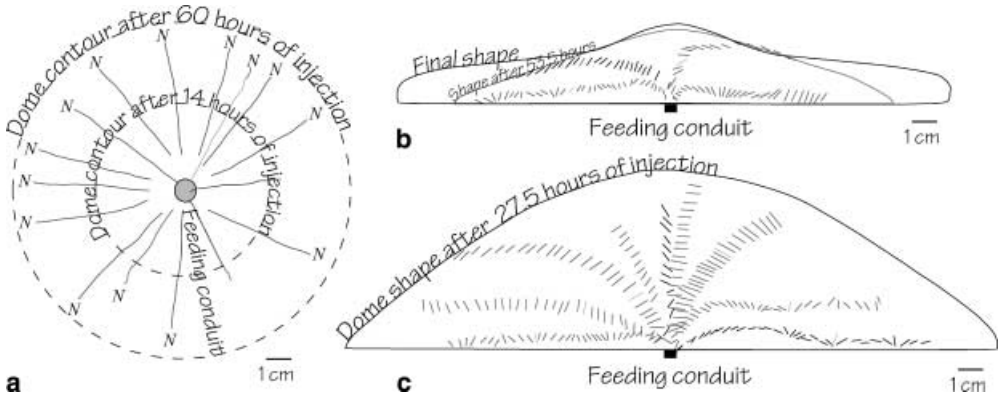

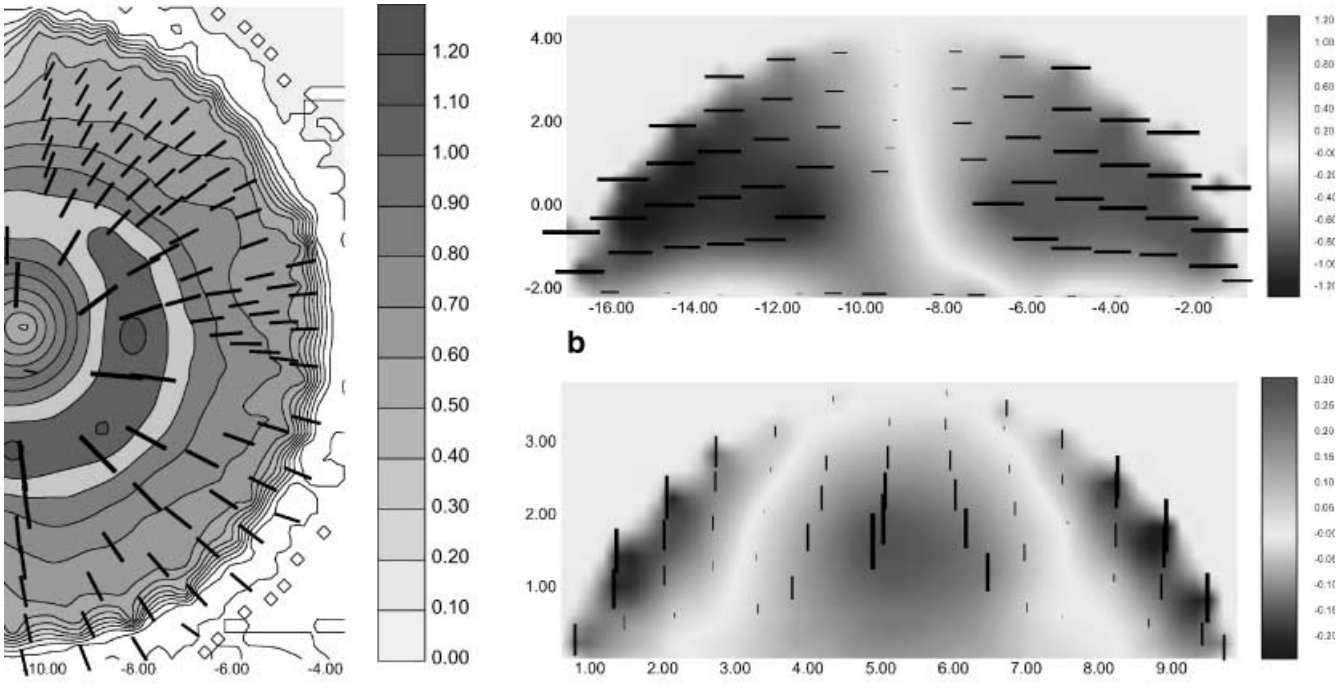

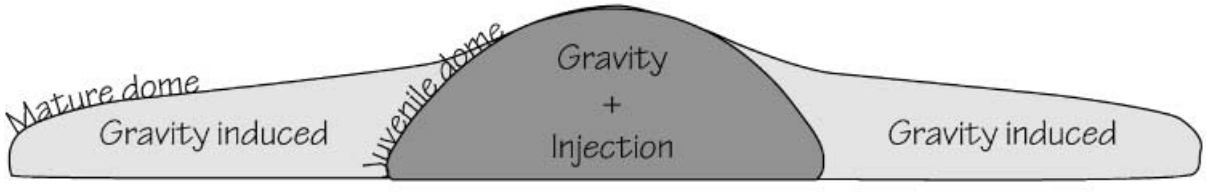

Fig. 5a, b Pattern of displacement. **a** Top view showing radial displacement in experiment 4. The so-called N paths correspond to a selected set of individual particles that have not reached the front yet at the end of the experiment. **b** Vertical section in experiment 9. Successive positions of sugar particles show parabolic trajectories symmetric on either side of a central vertical line. **c** Similar pattern of particle paths in experiment 10

Fig. 6a–d Displacement maps obtained from the deformed grid of experiments at 2.6 $cm^3\ h^{-1}$. **a** Top view showing radial translation vectors after 7 h of injection in experiment 20. **b**, **c** Vertical sections showing the horizontal (*top*) and vertical (*bottom*) components of displacements after 270 min of injection in experiment 15. **d** Conceptual sketch showing the shape evolution from juvenile to mature dome. The central zone is dominated by the injection force whereas the lateral sides are gravity induced

Displacement

Displacement vectors through time (XZ, X and Z), can be calculated for each node of the square grid from successive photos taken during experiments. Different maps corresponding to successive stages of deformation can be drawn where the total displacement vector as well as its horizontal and vertical components are visualised with different colours. Small bars parallel to the flow direction and that have a length proportional to the magnitude of displacement are added to some individual

points. Iso-displacement curves also can been drawn. Because the time between each photo is known, it is easy to calculate the velocity in any part of the dome between two intervals of time.

Total displacements for our experiments are represented in plan-view, in colours varying from yellow to red according to the displacement increase (Fig. 6a). In cross section, the origin is located at the base and centre of the model. For horizontal displacement maps, blue and red colours correspond to left- and right-directed displacement, respectively (Fig. 6b). Similarly, for vertical displacement maps, downward and upward movements are blue and red, respectively. Yellow indicates motionless areas (Fig. 6c).

Plan-view displacement vector maps confirm both that radial displacements occur with time and that velocities decrease from the vent to the margins of the dome (Fig. 6a). In vertical cross sections, horizontal displacement maps show the remarkable symmetry of particle paths on both sides of a vertical line of no displacement located above the feeding conduit (Fig. 6b). This pattern remains unchanged whatever the effusion rate.

Vertical displacement maps in cross sections confirm the interpretation inferred from the particle paths: a central zone where the material moves upwards and the lateral zones, symmetrical on either sides of the central one, where the material moves downwards (Fig. 6c). Between these two domains, a line can be drawn with no vertical motion. These observations, which confirm earlier assumptions (e.g. Fink 1978), are consistent with the fact that the central zone results from the competition between gravity and vertical injection whereas the surrounding domain is gravity induced.

A temporal analysis has been carried out comparing maps for successive stages of deformation. This analysis shows that, once the lateral zone develops, the shape of the central zone remains unchanged and does not evolve any more. This makes it possible to distinguish two stages in a dome's formation. A dome can be termed juvenile as long as the central zone has not taken its efinitive shape. A dome becomes mature once the central zone has achieved a stable configuration and is surrounded by a growing gravity domain (Fig. 6d).

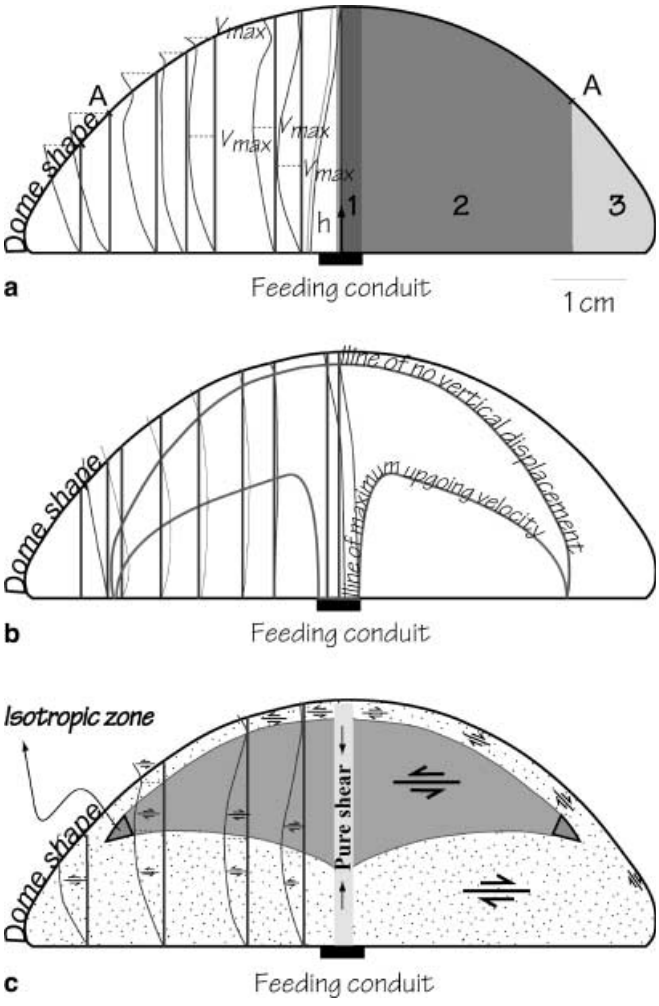

Fig. 7a–c Velocity gradients and shear senses in vertical sections as deduced from experiment 15, 270 min after grid emplacement. **a** Vertical velocity profiles. **b** Representation of the vertical components of velocity vectors. Deviation to the right and left from the initially vertical line indicate up-going and down-going vertical movement, respectively. **c** Vertical profiles for the horizontal component of velocity vectors and the resulting distribution of shear senses within the dome

Velocity gradients and shear senses

Velocity vectors in cross sections can be obtained from the deformed grids. Displacement vectors of each node of the deformed grid are recorded from successive photos taken during experiments. Because the interval of time is the same for all displacement vectors, we can calculate velocities throughout the model for different stages of deformation. Each velocity vector can be split into its horizontal and vertical components.

The velocity vectors allow three different zones in the dome to be distinguished (Fig. 7a). In zone 3, the velocity vectors are similar to those usually observed in materials spreading under their own weight and where displacement occurs with a coherent contact allowing no slip along the base. Velocity is zero at the base and increases toward the upper free surface of the dome. In contrast, in zone 1 located above the feeding conduit, the velocity is maximum at the base and decreases to zero at the upper free surface. These two domains are separated by a transitional zone (zone 2 on Fig. 7a) where the velocity vectors reveal a shape of a semi-amphora. The velocity is zero at the base of the model and increases until reaching a maximal value in the dome interior. Then, it decreases to a minimum value before increasing again to the upper free surface (Fig. 7a).

The injection force is balanced by gravity throughout the model producing this change in velocity pattern from zone 1 to 3. This is characterised by the appearance of a low velocity area just below the top free surface of the dome. This area of low velocity can be interpreted as

the place where the effects caused by gravity (sinking movement) and injection (rising movement) are in equilibrium. As expected, vertical motion is negligible in this area (Fig. 7b) where horizontal displacements prevail.

Along a set of selected vertical profiles, two lines can be defined from the vertical components of velocity vectors: a line of no vertical displacement and a line of maximum rising vertical velocity (Fig. 7b). Above the line of no vertical displacement, all particles move down because of the prominent effect of gravity. Below the line of maximum velocity, ascending material shows the prominent effect of injection. Between both, an intermediate zone undergoes rising motion, but with decreasing velocity (compare with Fig. 6c). This merely indicates that gravity progressively overcomes injection to cause rapid slowing down of the ascending particles (Fig. 7b).

Vertical velocity profiles obtained from the horizontal component of velocity enable us to determine the distribution of horizontal shearing deformation throughout the dome (Fig. 7c). On both sides of a vertical zone passing through the aperture, these velocity profiles reveal a central area with an inward sense of shear sandwiched by outward senses of shear. This change in the sense of shear merely results from a change in the sign of the velocity gradient with respect to the lower and upper zones.

Two lines of no shear strain constitute the upper and lower boundaries of this intermediate domain of reverse shearing sense. Towards the dome margins, the vertical velocity profile is concave, revealing an outward sense of shearing from bottom to top.

Stretch trajectories and strain intensity

Internal strain within the dome is reconstructed from the deformation of the square grid placed on the silicone. As the grid is made of circles inscribed in squares, strain can be computed both from deformed squares and deformed circles (see Fig. 2c).

Circles are transformed into elliptical shapes, which indicate the long axis (λ_1) of the strain ellipse (Fig. 8a). This principal axis should correspond to the attitude of flattening planes in vertical cross sections. This also enables us to determine the strain intensity throughout the model (Fig. 8b). Likewise, deformation of vertical and horizontal lines of the square grid makes it possible to reveal the strain pattern (Fig. 8c). Both methods reveal a similar strain pattern.

Horizontal lines are strongly bent upward in the centre of the dome and slightly downward towards the two margins. This is consistent with rising movement above the feeding conduit and sinking movement at the margin. This overall change in vertical motion within the model creates a component of vertical shear strain (Fig. 8c).

Stretch trajectories reveal a remarkable concentric stretching pattern in the central part. On either side of this concentric stretching zone, the triple junction between stretch trajectories defines an isotropic point in the strain field (Brun 1983; Fig. 8a).

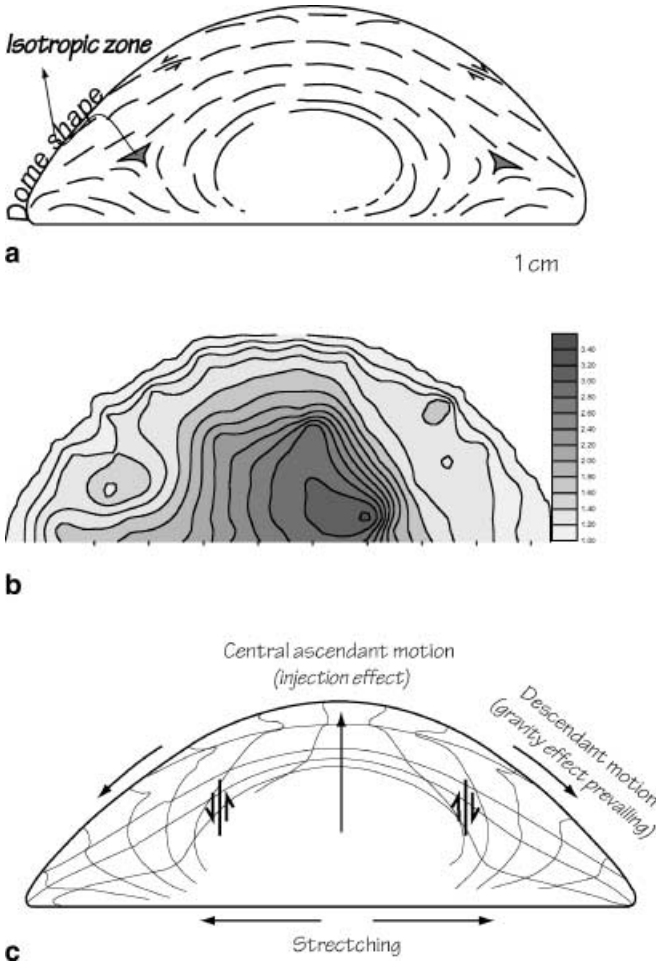

Fig. 8a–c Strain pattern from experiment 15 as deduced 270 min after grid emplacement. **a** Attitude of flattening planes. **b** Strain intensity. **c** Deformation of horizontal and vertical lines

The deformed grid from bottom to top above the feeding conduit reveals that the strain approximates pure shear (corresponding to vertical shortening and horizontal lengthening) because rectilinear lines of the initial grid remain nearly perpendicular after deformation (Figs. 7c and 8c). Away from this narrow central zone, the strain is a complex combination of simple shear and pure shear components (Fig. 8c).

The highest strain zone is located above the feeding conduit and matches the zone of maximum velocity and displacement. The strain decreases from this lower central zone, both to the upper free surface and the lateral sides of the model (Fig. 8b).

Natural examples

Data on internal strain in vertical cross sections of natural examples are relatively scarce as the interior of a deforming dome is not accessible to direct observations. To get strain data in natural examples, old domes partly removed by erosion must be studied. Again, vertical cross

a

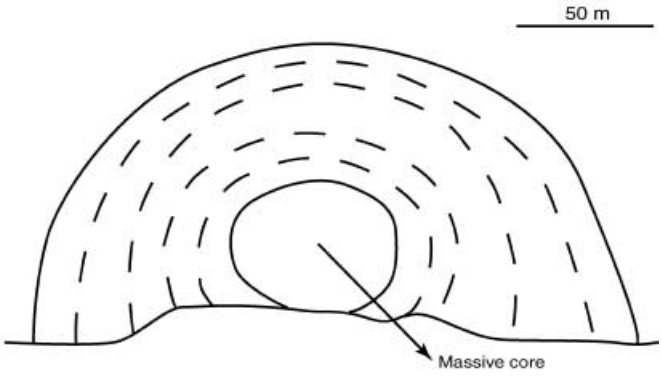

b

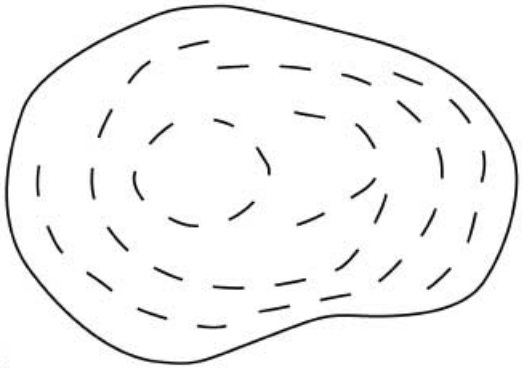

c

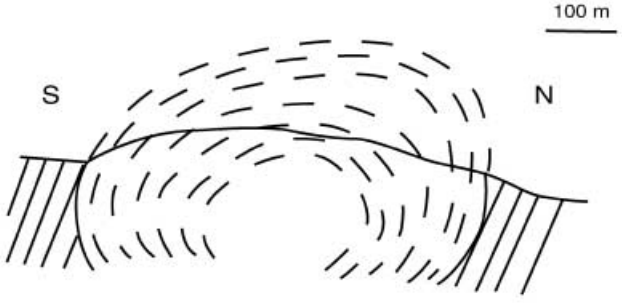

d

Fig. 9a–d Natural examples. **a** Concentric structures in a dome of Lipari Island (photography in Williams and McBirney 1979). **b** Concentric structure in the Mono-iwa dacitic dome on the Rebun Island in Japan (from Goto and Macphie 1998). **c**, **d** Map view and cross section of the concentric structure in a phonolitic dome of the French Massif Central (from Varet 1971)

sections are not very abundant explaining the lack of detailed strain analysis.

There are a few locations around the world where good exposures allow a comparison with the trajectories of the flattening plane observed in experiments. Some of these are the Raker Peak of Lassen Volcanic National Park in California (Macdonald 1972), domes in the French Massif Central (Varet 1971), domes on the Lipari Island in Italy (William and MacBirney 1979; Cas and Wright 1987) and the Mono-Iwa dome on the Hokkaïdo Island in Japan (Goto and Macphie 1998).

All authors have described a well-defined concentric planar structure in vertical sections of the domes (Fig. 9). There is not complete agreement among these authors about the significance of this concentric structure, but it is always described as a banding that pre-dates the cooling of the domes because it is frequently cross cut by well-identified prismatic columns. The concentric structure is then considered as being generated during the emplacement of the dome (e.g. Varet 1971; MacDonald 1972; Williams and McBirney 1979). In some cases, the flow lines in the dome are reconstructed as being perpendicular to the concentric planar structure (Fig. 9; Varet 1971).

In a more recent study, it has been demonstrated from a detailed analysis of microshear zones and crystal alignments that the banding observed in a Japanese dome is a plane of flattening. This flattening plane has a dome-like distribution analogue to the concentric planar structure observed in other domes.

Experiments shown in this paper confirm this interpretation. The deformed grids reveal that the flattening plane is concentric and matches the concentric planar structure described in natural domes. Because the distribution of the flattening plane in experiments merely results from particle paths that are parabolic and symmetric on both sides of a vertical line located above the feeding conduit, it is argued that the concentric planar structure in natural domes results from a similar process.

A study of the Hradiste dome in Bohemia has revealed inward senses of horizontal shear, which are opposite on both flanks of the dome (see Fig. 7 in Jancuskova et al. 1992). This was interpreted as resulting from successive intrusions of sheets of trachyte magma. From our experimental study, an alternative interpretation may be proposed in which inward shear senses are caused by vertical velocity gradients during dome growth.

Further qualitative and quantitative field studies are needed to make a useful comparison between nature and experiments because there is not enough data concerning strain intensities, strain regimes or shear senses within natural domes. Experimental results provided herein should be seen as a first proposition to be confirmed in the field or by theoretical studies.

Conclusion

The main results of this experimental study on strain in lava dome are as follows:

1. The overall geometry for a mature dome results from the balance between injection, which forces upward movements and generates a prominent upper central zone, and gravity, which forces downward movements and generates the flat-lying lateral margins. It follows that domes have inner and outer zones in which flow directions, strain patterns and strain rates differ significantly.
2. In vertical cross sections, motion trajectories are parabolic and symmetric on both sides of a vertical line located above the feeding conduit.
3. Vertical profiles for horizontal velocities throughout the model reveal an inward sense of shear in the central part of the dome.
4. In cross section, the attitude of flattening planes is remarkably concentric and displays two striking isotropic points next to the periphery of the dome.

Acknowledgements We are indebted to Stephen Blake and Jonathan Fink for thoroughly reviews, which helped to greatly improved the first version of the manuscript.

References

Anderson SW, Fink JH (1990) The development and distribution of surface textures at the Mount St Helens Dome, In: Fink JH (ed) Lava flows and domes, vol 2. IAVCEI Proceedings in Volcanology. Springer, Berlin Heidelberg New York, pp 25–46

Blake S (1990) Viscoplastic models of lava domes. In: Fink JH (ed) Lava flows and domes, vol 2. IAVCEI Proceedings in Volcanology. Springer, Berlin Heidelberg New York, pp 88–126

Brun JP (1983) Isotropic points and lines in strain fields. J Struct Geol 5(3/4):321–327

Bucher WH (1956) Role of gravity in orogenesis. Geol Soc Am Bull 67:1295–1318

Cas RAF, Wright JV (1987) Volcanic successions: modern and ancient. Chapman and Hall, London

Christiansen, Lipman (1966) Emplacement and thermal history of a rhyolite flow near Fortymile Canyon, southern Nevada. Geol Soc Am Bull 77:671–684

Cole JW (1970) Structure and eruptive history of the Tarawera Volcanic complex, NZ. J Geol Geophys 13:879–902

Dadd KA (1992) Structures within large volume rhyolite lava flows of the Devonian Comerong volcanics, southern Australia, and the Pleistocene Ngongotaha lava dome, New Zealand. J Volcanol Geotherm Res 54:33–51

Duffield WA, Dalrymple GB (1990) The Taylor Creek Rhyolite of New Mexico: a rapidly emplaced field of lava domes and flows. Bull Volcanol 52:475–487

Fink JH (1978) Surface structures on obsidian flows. PhD Thesis, Stanford University, Stanford, California

Fink JH, Bridges NT (1995) Effects of eruption history and cooling rate on lava dome growth. Bull Volcanol 57:229–239

Fink JH, Griffiths RW (1990) Radial spreading of viscous-gravity currents with solidifying crust. J Fluid Mech 221:485–509

Fink JH, Manley CR (1987) Pumiceous and glassy textures in rhyolite flows and implications for eruption and emplacement. Geol Soc Am Spec Pap 212:77–88

Goto Y, Macphie J (1998) Endogenous growth of a Miocene submarine dacite cryptodome, Rebun Island, Hokkaido, Japan. J Volcanol Geotherm Res 84:273–386

Griffiths RW, Fink JH (1993) Effects of surface cooling on the spreading of lava flows and domes. J Fluid Mech 252:667–702

Griffiths RW, Fink JH (1997) Solidifying Bingham extrusions: a model for the growth of silicic lava domes. J Fluid Mech 347:13–36

Hubbert MK (1937) Theory of scale models as applied to the study of geologic structures. Geol Soc Am Bull 48:1459–1520

Huppert HE, Sheperd JB, Sigurdsson H, Sparks RSJ (1982) On lava dome growth, with application to the 1979 lava extrusion of the Soufriere of St Vincent. J Volcanol Geotherm Res 14:199–222

Jancuskova Z, Schulmann K, Melka R (1992) Relation entre fabriques de la sanidine et mise en place des magmas trachytiques (exemple du massif de Hradiste, Bohême du nord). Geodynam Acta 5:235–244

Lejeune AM (1995) Evolution of lava domes: experiments using gum rosin, a new analogue for magmas. EOS Suppl 76-46:680

Macdonald GA (1972) Volcanoes. Prentice Hall, Englewood Cliffs

Merle O (1986) Pattern of stretch trajectories and strain rate within spreading–gliding nappes. Tectonophysics 124(3/4):211–222

Merle O (1998) Internal strain within lava flows from analogue modelling. J Volcanol Geotherm Res 81:189–206

Merle O, Borgia A (1996) Scaled experiments of volcanic spreading. J Geophys Res B6 101:13805–13817

Miller TP (1994) Dome growth and destruction during the 1989–1990 eruption of Redoubt Volcano. J Volcanol Geotherm Res 62:197–212

Murase T, McBirney AR, Melson WG (1985) Viscosity of the dome of Mount St. Helens. J Volcanol Geotherm Res 24:193–204

Nakada S, Miyake Y, Sato H, Oshima O, Fujinawa A (1995) Endogenous growth of dacite dome at Unzen volcano (Japan) 1993–1994. Geology 23(2):157–160

Ramberg H (1981) Gravity, deformation and the Earth's crust. Academic Press, London

Swanson D, Holcomb RT (1990) Regularities in growth of the Mount St Helens dacite dome, 1980–1986. In: Fink JH (ed) Lava flows and domes. IAVCEI proceedings in volcanology, vol 2. Springer, Berlin Heidelberg New York, pp 3–24

Swanson D, Dzurisin D, Holcomb RT, Iwatsubo EY, Chadwick WW Jr, Casadevall TJ, Ewert JW, Heliker CC (1987) Growth of the lava dome at Mount St Helens, Washington (USA) 1981–1983. Geol Soc Am Spec Pap 212:1–16

Varet J (1971) Structure et mise en place des massifs phonolitiques du Cantal (Auvergne, France). Geol Rundsch 60(3):948–970

Williams H (1932) The history and character of volcanic domes. Univ Calif Geol Sci 21:51–146

Williams H, MacBirney AR (1979) Volcanology. Freeman, Cooper and Co, San Francisco